The Permeability of Novel Hybrid Fiber Composite Material for Use as Diesel Particulate Filters

*Alastair J. Houston, Douglas Boubert, and Trevor William Clyne**

An investigation is presented into modeling of gas flow through particle/fiber hybrid composite materials designed for use as diesel particulate filters (DPFs). The work leads to the creation of a modified version of the Carman–Kozeny equation, specifically tailored for such structures. Details of computational fluid dynamics (CFD) simulation of gas flow through modeled structures are provided, leading to formulations to account for the loss of surface area associated with sintering and a tortuosity effect dependent on the porosity level. Based on these outcomes, a simple analytical expression is derived, and it is shown that predicted permeability values obtained with it are in good agreement with experimental data.

1. Introduction

1.1. Use of Hybrid Composite Material for DPFs

Diesel particulate filters (DPFs) are an essential component of diesel engines, particularly for road vehicles. They are often used in conjunction with diesel oxidation catalysts (DOCs), which help to control gaseous emissions and have been mandatory[1] on all new diesel cars sold in Europe since 1998. DPFs, which first entered series production[2] in 2000, are designed[3] to reduce substantially the emission of particulate matter (PM) in the coarse (1–10 μm), accumulation (0.1–1 μm), and nuclei (<50 nm) categories of size. The PM is largely carbon, although trace levels of various elements and compounds are also present.[2]

The current basic design of a DPF is a ceramic extruded cylindrical structure, containing a square "honeycomb" of parallel channels in the axial (exhaust) direction. Adjacent channels are alternately plugged at each end, forcing the exhaust gases to flow through the porous substrate walls, which mechanically traps the PM.[1,3] The wall material must be highly permeable to maintain a low exhaust back pressure (EBP), but it must also have a high filtration efficiency, so the PM becomes trapped.[4] The filter captures particles via physical impact and retains them until removal (oxidation to gas) via active or passive regeneration. A typical specific permeability of a current DPF material[2] is about 10^{-2} m².

Most current DPFs are made by (incomplete) sintering of coarse cordierite or silicon carbide particles, so as to create a highly porous structure. This work is focused on a "hybrid" composite material incorporating both (relatively fine) fibers and (coarse) particulate, which has recently been proposed[5] as a candidate DPF material. The presence of the fibers has been shown[5] to provide enhanced thermal shock resistance and is likely to offer improved filtration characteristics and retention capacity for PM extracted from the exhaust. Part of the basis for such performance enhancement is that it incorporates multiscale pore architecture, allowing easy gas flow through large pores and fine-scale filtration of PM via smaller channels within fiber bundles.[6]

There is, thus, interest in predicting how the relevant characteristics of a filter made of such material will depend on the proportions of fibers and particles, and on the porosity level. While the filtration properties of structures composed entirely of particles[7–9] and entirely of fibers[10] have been widely studied, this has not been done previously for such hybrid composites.

1.2. The Carman–Kozeny Equation

The most commonly used equation for assessing the permeability for fluid flow through porous media is that of Carman–Kozeny.[11,12] It can be derived by simplifying the pore structure into a regularly spaced set of cylindrical channels, with equivalent surface area and porosity, applying the Hagen–Poiseuille equation for fluid flow through pipes, and then substituting the resulting pressure gradient into Darcy's equation. In its simplest form, the Carman–Kozeny equation can be written as

$$\kappa = \frac{p^3}{\lambda S^2} \tag{1}$$

where κ is the permeability (m²), p is the porosity, S is the specific surface area (m² m⁻³), and λ is a dimensionless parameter (related to the channel tortuosity), which is often assumed[12] to have a constant value of about 5.

Dr. A. J. Houston, Prof. T. W. Clyne
Department of Materials Science and Metallurgy
Cambridge University
27 Charles Babbage Road, Cambridge CB3 0FS, UK
E-mail: twc10@cam.ac.uk

Dr. D. Boubert
Magdalen College
High Street, Parks Road OX1 4AU, UK

ⓘD The ORCID identification number(s) for the author(s) of this article can be found under https://doi.org/10.1002/adem.202000562.

This equation gives a good indication of the permeability in many cases, although it was originally focused on flow through fluidized beds composed of packed particles. In fact, there have been numerous investigations[7–10,13,14] into how it should be modified (mainly in terms of the value of the dimensionless constant) for different geometries, including assemblies of spherical particles with a range of sizes.[7–9] There have also been investigations covering transverse flow through a set of aligned fibers[13] and flow characteristics in other fibrous and highly anisotropic structures.[10,11] A recurrent concern is that, in practice, the value of the constant may be dependent on the porosity level (for a given type of geometry), as well as on the geometry itself.

This work is aimed at identifying a form of the Carman–Kozeny equation that is suitable for highly porous hybrid composite material containing both fibrous and particulate constituents. While porosity can easily be measured, much more effort is required to obtain an accurate experimental value for the specific surface area. There is, thus, considerable interest in deriving an analytical equation with a capability for prediction of the permeability of such a hybrid composite filter, given its porosity, fiber/particle proportion, and the dimensions of individual particles and fibers.

2. Modeling of Gas Flow

2.1. Domain and Mesh Generation

MATLAB was used to generate random distributions of particles and fibers. Each particle was specified in terms of the Cartesian coordinates of its center and a radius. Each fiber required six parameters—three for the coordinate of one end and a further three to specify the orientation. To minimize the number of parameters, all particles in a model had the same radius, and all fibers had the same length and radius. This neglects any effects of surface roughness or fiber curvature, although the latter is not expected to affect the permeability of a fibrous medium.[10]

For each generated structure, it is useful to identify the volume fractions of fibers, f, and voids (i.e., the porosity), p. The remaining volume is occupied by particles. Of course, these three values must sum to 100%. A further useful parameter is b, the fiber solid fraction, defined by

$$b = \frac{f}{(1 - p)} \tag{2}$$

such that $b = 0$ defines a porous structure containing only particles, and $b = 1$ defines a porous structure containing only fibers. The MATLAB script used to create the structures functioned by calculating the number of spheres and cylinders required to make the best approximation of a specified fiber solid fraction, b, and porosity, p, within a predetermined cubic volume (building block).

The particles were inserted first, followed by the fibers. The addition of each constituent was carried out using randomly generated coordinates. Whether a particle or fiber was accepted depended on certain criteria being met. Particles were accepted provided they did not exceed a predetermined maximum allowed overlap (set to be 2 μm) with other particles already present. Fibers were added, so that a degree of overlap with existing particles or

fibers was necessary—representing a requirement for some sintering to have occurred. Fiber orientation was based on three randomly generated numbers, defining a direction in Cartesian space, measured from the origin. The chosen point was required to lie within a unit sphere centered on the origin, such that there is no bias in fiber orientation. However, the degree of overlap was still limited to the same maximum of 2 μm. During this procedure of filling the volume with spheres and cylinders, periodic boundary conditions were maintained in all three principal directions. There was, thus, always an integral number of both fibers and particles within the building block of the model.

Larger numbers of parameters were needed for high fiber fractions—the small size of the fibers compared with the particles means that more of them are needed to give a certain porosity level, and also, they require more parameter values than particles. Analysis was, therefore, limited to the fiber solid fraction (b) values of 0.5 or less. For selected models, the coordinates of all the spheres and cylinders were imported into COMSOL using the application builder feature. At this point, a typical imported model would appear, as shown in **Figure 1**, containing all fibers and particles that intersect with a central 50 μm cube "building block." The structure of fibers and particles has a 50 μm repeating distance in all three of the principal directions, most clearly observed by the regular distribution of the particles, as two intersecting simple cubic structures.
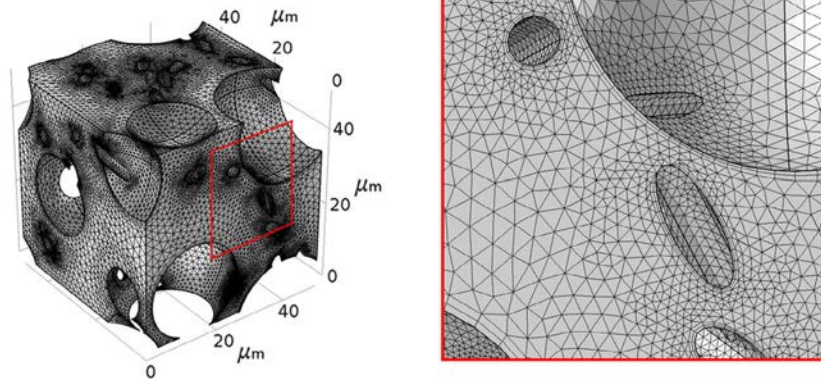
In terms of fluid flow, the region of interest is the air space between the assembly of fibers and particles. It was, therefore, necessary to create the inverse of this structure. A block of the same dimensions of the cube of interest was added to the geometry, and the spheres and cylinders were subtracted from this volume. A mesh could then be generated automatically. Such a mesh is shown in **Figure 2**, where the periodic boundary conditions are also evident.

2.2. Permeability Evaluation

With a generated structure of this type, the permeability can be evaluated in two ways. First, it can be obtained via a COMSOL
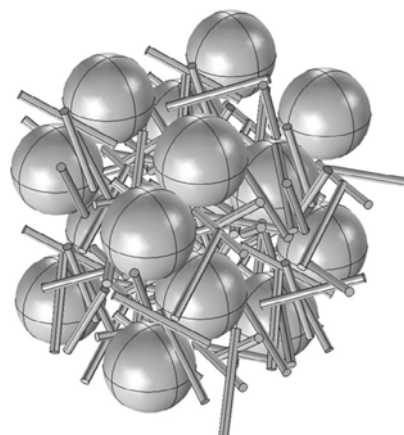
Figure 1. Depiction of a typical modeled structure, the repeat unit being a 50 μm cube, intersected by 30 μm diameter spheres and fibers of length 30 μm and diameter 3 μm. In this case, the porosity is 62.6%, and the fiber volume fraction is 10%.

**ADVANCED
SCIENCE NEWS**
www.advancedsciencenews.com

**ADVANCED
ENGINEERING
MATERIALS**
www.aem-journal.com

Figure 2. Finalized mesh of air volume (50 μm cube), viewed from within the assembly of particles and fibers in Figure 1. The volume has periodic boundary conditions, and in this case, boundary layers were present.

simulation of fluid flow through it. By assuming laminar flow, and assigning one face to be the inlet, the opposite face to be the outlet, and allowing continuity over the other four faces, the permeability can be calculated directly in COMSOL, solving the Navier–Stokes equations to obtain the steady-state flow field. For each volume, initial conditions were set, such that there was a constant gas inlet velocity of $0.1 \, \text{m s}^{-1}$. The outlet was set to have 0 Pa pressure, such that the average pressure on the inlet face would be a direct measure of the back pressure across the volume. The permeability can be measured in this way for three orthogonal directions, normal to the faces of the cube.

The second method involves using the Carman–Kozeny equation (Equation (1)). In the created model, the values of porosity and specific surface area are known precisely, and so, by taking λ to have a value[12] of 5, the permeability can be obtained by substituting in the equation.

2.3. Analytical Treatment of Permeation

While the abovementioned procedure allows Carman–Kozeny to be used to predict the permeability of the model, the precise value of the specific surface area, S, is often unknown for a real material (filter). Hence, there is interest in being able to obtain S from information that can be readily obtained, such as the fiber and particle sizes and the proportion of the two (expressed as the fiber solid fraction, b).

In the model, if there is no overlap between any of the spheres and cylinders, the specific surface area will be given by

$$S = \frac{n_s A_s + n_c A_c}{V_T} \qquad (3)$$

where V_T is the total volume of the cube, n_s and n_c are the numbers of spheres and cylinders in the volume, and A_s and A_c are the surface areas of a single sphere and a single cylinder. As n_s and n_c are the integers for this model, the two values can be expressed in terms of the fiber solid fraction, b, and the porosity, p

$$b = \frac{n_c V_c}{n_s V_s + n_c V_c} \qquad (4)$$

$$1 - p = \frac{n_s V_s + n_c V_c}{V_T} \qquad (5)$$

Rearranging to obtain expressions for n_s and n_c, and substituting these into Equation (4), writing the areas and volumes of spheres and cylinders in terms of their linear dimensions (D_s, D_c, and L for the diameter of the spheres, diameter of the cylinders, and length of the cylinders, respectively) and ignoring any overlap, leads to

$$S = (1 - p)\frac{6(1 - b)}{D_s} + \frac{4b}{D_c} + \frac{2b}{L} \qquad (6)$$

This expression can then be substituted back into Equation (1) to obtain a predicted relationship among permeability, porosity, and fiber content, dependent on the size parameters of the sphere and cylinder components (D_s, D_c, and L).

2.4. Correction Terms

As noted earlier, this expression for the specific surface area (Equation (6)) does not account for any overlap. During the model generation, new components were added, provided the overlap did not exceed a prescribed level, leading to a highly interconnected final structure as a model for sintering. Each occurrence of an overlapped region will cause a reduction in surface area. Equation (6) will, thus, always give an overestimate for S. The significance of this effect will be greater for lower porosities and higher fiber fractions, which are associated with higher degrees of overlap.

A further assumption incorporated into the Carman–Kozeny equation, as expressed by Equation (1), concerns λ, the dimensionless tortuosity constant. While often taken to be equal to 5, it is sometimes ascribed a different value. In fact, a value of λ can be obtained for a model of this type, because both porosity and surface area are known, and the permeability can be obtained via fluid flow simulation in COMSOL. Any dependence of the value of λ on porosity or fiber fraction can, thus, be ascertained.

Various particle and fiber sizes were studied, as shown in **Table 1**. These sizes are representative of material produced in the previous study.[5] All of these cases can be used to find

ADVANCED
SCIENCE NEWS
www.advancedsciencenews.com

ADVANCED
ENGINEERING
MATERIALS
www.aem-journal.com

Table 1. Combinations used for fiber diameter and length, and particle diameter.

Fiber diameter [μm]	Fiber length [μm]	Particle diameter [μm]
3	30	30
4	30	30
5	30	30
3	15	30
3	35	30
3	30	20
3	30	10

the most appropriate correction in one optimization step, rather than analyzing each data set individually and attempting to find a common solution between them. Using a statistical approach also allows for clear visualization of whether the additional corrections are justifiable, or are adding unnecessary complication to the model.

The analysis used to evaluate the correction factors was the Markov chain Monte Carlo (MCMC) method. For both specific surface area and tortuosity terms, additional variables were introduced, corresponding to linear dependencies in both porosity and fiber fraction. These variables started with uniform prior values, with the distribution of their values being calculated by random sampling in probabilistic space. In such a method, for two sets of parameters, the best set is added to the chain of parameter values with a certain probability, determined by how much better it is—this is termed a Markov chain. The effectiveness of a pair of parameters was evaluated via Gaussian probabilities to obtain the best prediction of the permeability, assuming that the permeabilities calculated using COMSOL and a specific surface area were distributed normally about planes in porosity–fiber solid fraction (p–b) space. After iterating the process a number of times, a steady-state distribution can be found.

With so many additional degrees of freedom added, the fit of the model to the data can become very good. However, it became apparent that not all the additional variables were required. By systematically removing certain parameters, it was possible to identify those of significance.

3. Modeling Outcomes

3.1. Permeability

The permeability (measured via fluid flow simulations in COMSOL) of models with a range of porosity and fiber solid fractions is shown in **Figure 3**. In all these samples, the particle diameter, fiber diameter, and fiber length were kept constant at 30, 3, and 30 μm, respectively. The permeability is observed to vary significantly with both porosity and fiber solid fraction. The permeability scale is logarithmic, and so the full range of data spans almost two orders of magnitude.

As expected from the Carman–Kozeny equation, the permeability tends to be high at high porosities. In addition, the permeability is significantly affected by the fiber solid fraction, b, or expressed slightly differently, by the fiber volume fraction, f.
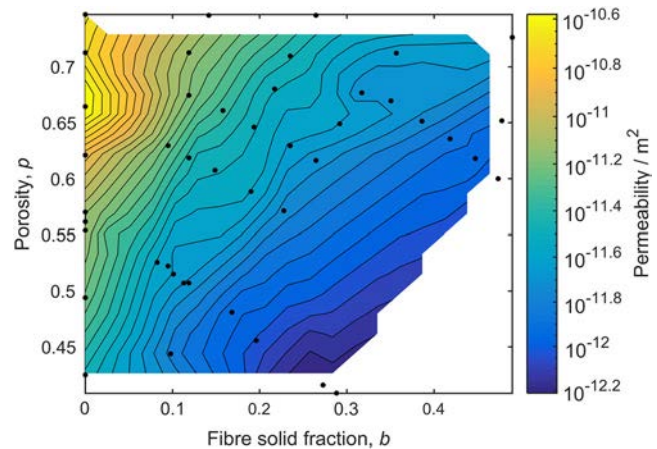
Figure 3. Contours of permeability, as a function of porosity, p, and fiber solid fraction, b, obtained via fluid flow simulations: modeling runs were carried out for all of the p–b combinations indicated by black markers.

As b (or f, at constant p) is increased, the permeability decreases. This is most significant as the first few fibers are added, but remains true at higher fiber fractions. The permeability values in all cases are comparable to values typical of commercial DPFs (around 10^{-2} m^2).

Substituting the expression for S with no overlap (Equation (6)) into the basic Carman–Kozeny (Equation (1)) and rearranging to obtain a relationship among porosity, permeability, and fiber solid fraction lead to

$$\sqrt{\frac{p^3}{\lambda \kappa (1-p)^2}} = b\left[\frac{4}{D_c} + \frac{2}{L} - \frac{6}{D_s}\right] + \frac{6}{D_s} \tag{7}$$

This function has units of m^{-1}. For a given size of fibers and particles, the right hand side of this equation increases linearly with b, as shown in **Figure 4**. Also plotted in Figure 4 are the values of the function on the left hand side (LHS) of Equation (7), using permeability values obtained in two different ways—via COMSOL simulations and from the Carman–Kozeny equation (using exact values of S for the models concerned and a value of 5 for λ). These are in good agreement.

The error bars on the COMSOL data reflect the variation obtained by measuring the permeability in the three orthogonal directions of a single volume. In view of the difficulty of accurate experimental measurement of S, Equation (7) offers a convenient way of estimating the permeability using only the porosity, fiber solid fraction, and fiber and particle sizes. However, it is shown in Figure 4 that, while the y-intercept of this line is approximately correct, the gradient is somewhat greater than it should be. This is expected, because the surface area loss due to overlap is being ignored, resulting in over-prediction of the gradient. Similar outcomes are obtained for all combinations of particle and fiber sizes listed in Table 1.

3.2. Reduction in Surface Area

As S can be obtained analytically for no overlap (using Equation (6)), and the actual specific surface area of a
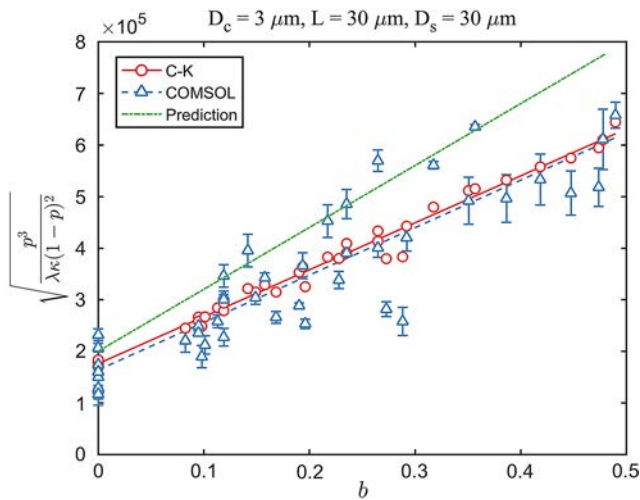
Figure 4. A plot of the function on the LHS of Equation (6) against fiber solid fraction, for the fiber and particle dimensions shown. Red circles represent permeability values obtained using flow simulations, whereas blue triangles correspond to those from Carman–Kozeny (Equation (1)), using exact values of porosity and surface area and a λ value of 5. The green line is a plot of Equation (7).
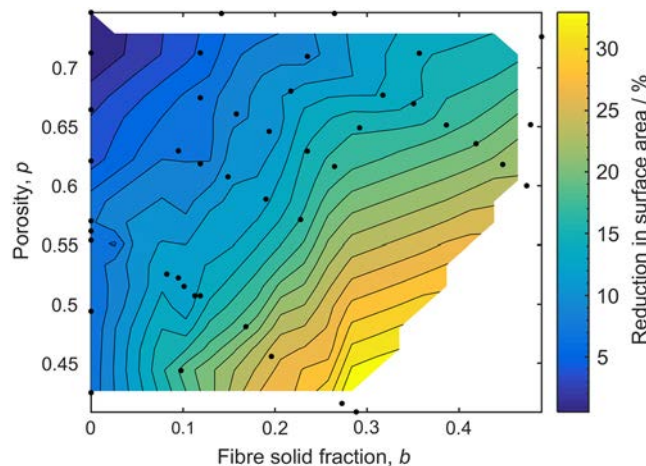
Figure 5. Contours of reduction in surface area due to overlap, as a function of the porosity, p, and fiber solid fraction, b, carried out via modeling runs for all the p–b combinations indicated by black markers.

COMSOL model can be calculated, the fraction of the calculated surface area that has been lost due to overlap can be estimated. **Figure 5** shows this effect of overlap over a range of porosity and fiber solid fraction values. At low fiber solid fraction and high porosity, the effect is not large and will not have a substantial effect on the predicted permeability. However, with low porosity and high fiber solid fraction, the reduction in surface area is significant, reaching as much as 30%. Such overlap levels will have a pronounced effect when predicting the permeability.

The degree to which this overlap affects the surface area will, of course, be a function of how much overlap is allowed within the model. In the initial model setup, the maximum allowed overlap was 2 μm. If this overlap was to be reduced, there would be a lower reduction in surface area and vice versa. The maximum value of 2 μm was selected as being representative of the degree of sintering expected to take place (when creating a highly porous structure of this type). This dependency on the allowed overlap means that the following analysis relates only to this specific case. However, the approach could be applied to other cases.

3.3. Kozeny Constant

Values of λ were obtained via Equation (1), by setting the permeability equal to that of simulation outcomes, and using precise values of porosity and surface area from the COMSOL model geometry. These values are shown as contours in p–b space in **Figure 6**. It can be seen that, while the commonly used value of 5 is not an unreasonable one, the most appropriate value for a given case could differ significantly from this. In particular, there is a clear tendency for smaller values to be required when the porosity level is relatively low ($<\approx$60–65%). The optimum value of λ in particular regimes is not easy to establish, although studies on transverse flow through parallel arrangements of fibers suggest that it should have a minimum value at porosities around 0.4–0.6, but higher values for both higher and lower porosities.[13,15,16]

As λ is often considered to be a measure of the degree of tortuosity of the flow path, this finding suggests that the fluid follows more tortuous paths through structures with higher porosity. This could be associated with a greater degree of interaction between fluid streams passing through more open structures—an effect that would be picked up by fluid-flow simulations, but not by simple geometrical arguments based on specific surface area, etc. There appears to be little effect of the fiber solid fraction on the optimum value of λ.

3.4. Corrections

In view of these results, corrections were made to both S and λ terms. The Kozeny constant, λ, was taken to be linearly
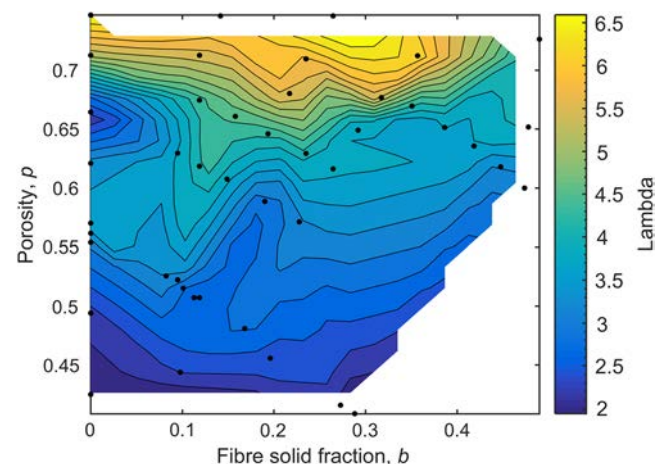
Figure 6. Contours of the value of the parameter λ, as a function of porosity, p, and fiber solid fraction, b, obtained via fluid flow simulations: such runs were carried out for all of the p–b combinations indicated by black markers.

2000562 (5 of 9)

ADVANCED
SCIENCE NEWS
www.advancedsciencenews.com

ADVANCED
ENGINEERING
MATERIALS
www.aem-journal.com

dependent on porosity, p, and two additional parameters were introduced, representing the gradient and the intercept of this linear relationship

$$\lambda = m_\lambda p + c_\lambda \tag{8}$$

The value of S was assumed to be linearly dependent on both p and b, resulting in three additional parameters. These were added to each term in the equation for S (Equation (6)), giving a total of nine additional degrees of freedom. Both were solved simultaneously using the MCMC method outlined in §2.4. Once solved, the fit of the model to the data was found to be very good. However, this was at the expense of adding many degrees of freedom. By systematic removal of parameters having little effect, it was found that only two of the nine associated with S were significant.[17] These were both associated with the cylinder diameter term, consisting of a constant offset term and a linear dependence on the porosity, p. As such, the correction term for the specific surface area (an additional term in Equation (6)) was found to be of the following form

$$(1-p)b\frac{m_{p,D_c}p + c_{D_c}}{D_c} \tag{9}$$

The results of the MCMC solution for the four new terms are shown in **Figure 7**. These terms are the constant and linear porosity dependence terms for λ and the constant and linear porosity dependence of the cylinder diameter term, designated c_λ, m_λ, c_{D_c}, and m_{p,D_c}, respectively. Also, shown in Figure 7 are standard deviation data for both S and κ (σ_s and σ_κ, respectively). Along the diagonal, the error in the value of any of the six parameters is normally distributed. The mean value and the positive and negative errors are provided above the histograms in each case. The scatter plots show the mutual interactions between the four additional parameters and the standard deviation of the values of S and κ. In all but two cases, the distributions are radially symmetric, with no skew. These are encouraging results, showing that the predicted mean values of the four new parameters correlate with the mean value of the standard deviation of the measured κ values about predicted planes of both S and κ. The absence of skew implies that there are sufficient data, and that the effects of the parameters are well captured by the data.

There are, however, two pairs of scatter plots that show significant dependency of two parameters on one another. The first pair relates to m_λ and c_λ, which are, respectively, the gradient and intercept of the dependence of λ on p. Some degeneracy (compensation for a fall in one by a rise in the other) between these two is unsurprising, because it is commonly observed for an intercept and gradient of a straight line being fitted to data with some scatter. A similar effect is observed for the two terms associated with the cylinder diameter. If it were assumed that there was no dependence of λ on porosity, then m_λ would be zero, and λ would have a constant value of c_λ. However, Figure 7 shows that m_λ is actually some way from zero, making it highly unlikely that λ has no dependence on p. The inclusion of a dependence of λ on p is, therefore, essential. This quantifies a trend that is clear on inspection of Figure 6.

Using the figures indicated in Figure 7, the most appropriate expression for λ is

$$\lambda = 8.1p - 1.14 \tag{10}$$

This leads to the apparently nonsensical outcome of negative values for λ when the porosity is very low ($<14\%$). This arises because the data set includes nothing with p values near that range. In fact, it would not be possible to create a structure with such a low porosity using the model being used, and such a structure is certainly of no interest for applications, such as DPFs, so this is not a cause for any concern.

Again, referring to Figure 7, the additional cylinder diameter correction term of S may be written

$$(1-p)b\frac{2.35p - 2.16}{D_c} \tag{11}$$

3.5. Final Expression

It follows that the final expression for the permeability may be written as

$$\kappa = \frac{p^3}{(8.1p - 1.14)(1-p)^2\left[\frac{6(1-b)}{D_s} + \frac{(1.84 + 2.35p)b}{D_c} + \frac{2b}{L}\right]} \tag{12}$$

This equation allows prediction of the permeability, κ, based on the porosity, particle and fiber dimensions, and proportion, b. Part of the denominator is Equation (10), which is the λ term (dependent only on porosity). The rest of the denominator is the surface area term (Equation (6)), including the correction to the cylinder diameter term (Equation (11)). This part of the equation highlights the effect of fiber content, b (or equivalently, f, at constant p), on the permeability. The addition of fibers, therefore, does not appear to greatly influence the tortuosity, but significantly increases the specific surface area.

To facilitate understanding of this equation, plots showing the dependence of this function on p (for three b values) and on b (for three p values) are presented in **Figure 8**. As p is raised, κ increases, as expected from the Carman–Kozeny equation. However, the dependence of κ on fiber solid fraction, for a constant porosity level, is also significant, with κ decreasing by an order of magnitude as b is raised from 0% to 50%.

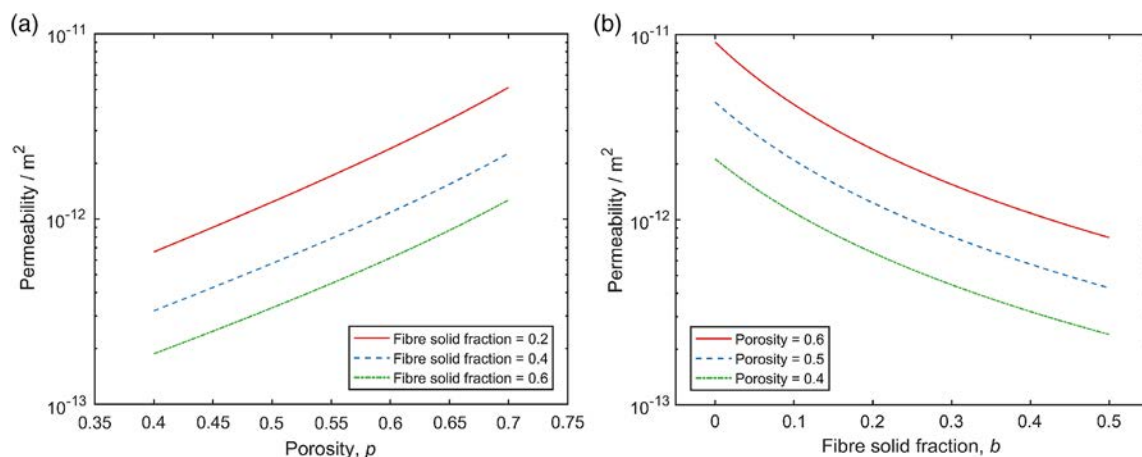## 4. Comparisons between Modeling and Experimental Outcomes

In practice, there are limitations on the p–b combinations that are possible. For example, using higher compaction pressures will reduce p, as will prolonged sintering or use of shorter fibers. It is in any event important to relate modeling outcomes to experimental results. Recent experimental work[5] on the effect of fiber solid fraction on porosity and permeability can be used to assess whether the sphere/cylinder model provides a good representation of actual flow characteristics. One approach to this is to use Equation (12) to create permeability contours in p–b space and then superimpose the measured p–b combinations of experimental material and check whether the measured permeabilities are in good agreement with the contours.
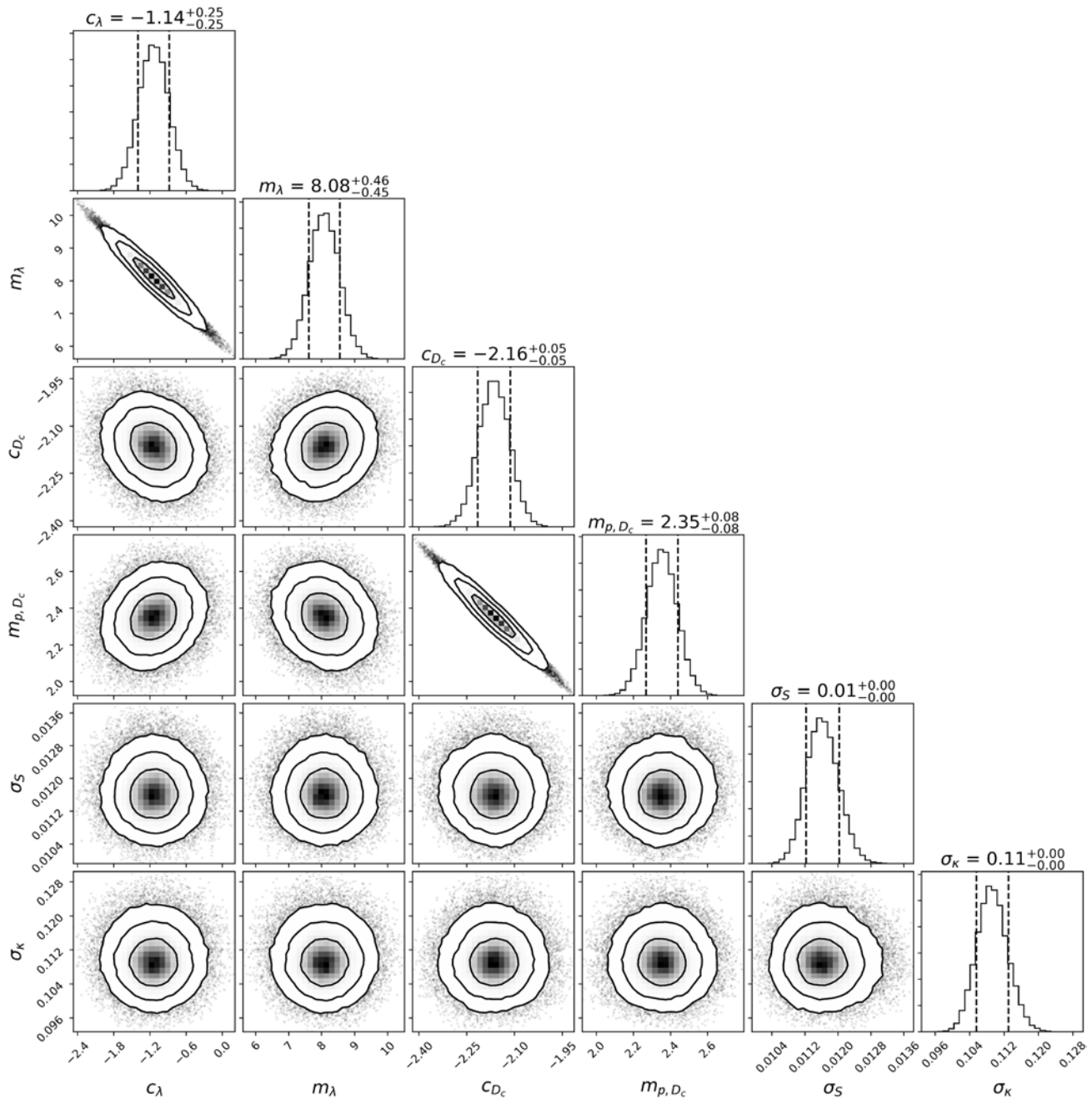
Figure 7. Probability distributions for the variables c_λ, m_λ, c_{D_c}, m_{p,D_c}, σ_S, and σ_κ, and the correlations between them.

Figure 9 shows such a contour plot, with five points superimposed that correspond to different materials, which were manufactured and then characterized in terms of p, b, and κ values. It can be seen that, while they cover a substantial range of b values, and a fairly wide range of porosity levels, the corresponding predicted (and indeed measured) values of κ do not vary so much. This simply reflects the practical difficulties of producing, say, high p–low b or low p–high b combinations. Nevertheless, agreement between model and experiment is good.

This is shown a little more clearly in **Figure 10**, which shows essentially the same comparison, but this time as a plot of permeability against b. The predicted value of permeability (solid red line) is obtained by calculating the permeability along the trend line of the data in Figure 9. One point worth noting about the predictions is that (fixed) values must be used for particle diameter, fiber diameter, and fiber length. These were measured experimentally (with standard deviations) to be 28 ± 12, 3.7 ± 1.0, and $37 \pm 10\,\mu$m, respectively. These deviations have been converted to error bands on the predicted permeability

ADVANCED
SCIENCE NEWS
www.advancedsciencenews.com

ADVANCED
ENGINEERING
MATERIALS
www.aem-journal.com

Figure 8. Plots of predicted permeability values as a function of p and b, obtained using Equation (12), for the case of $D_c = 3\,\mu m$, $D_s = 30\,\mu m$, and $L = 30\,\mu m$.
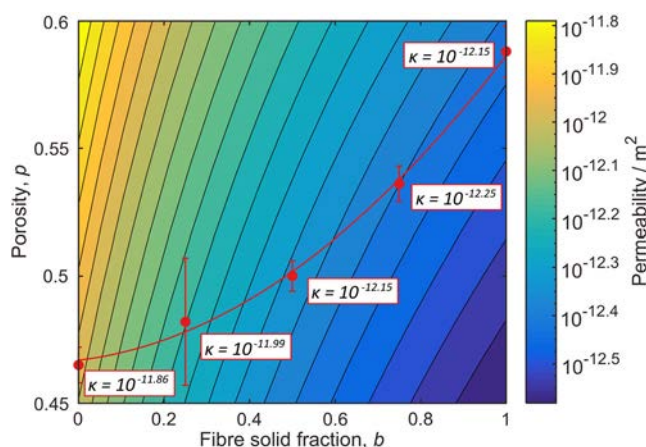
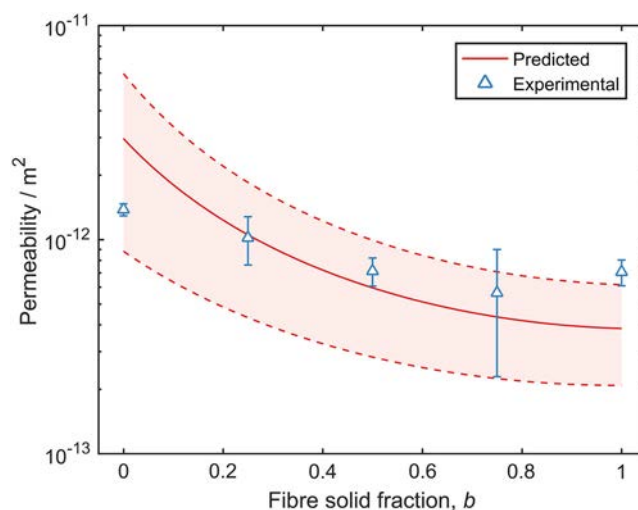

Figure 9. Contours of permeability in p–b space, generated using Equation (12), together with five superimposed points representing materials for which p and b, and also κ, were measured experimentally.[5]

Figure 10. Predicted (Equation (12)) and measured permeabilities, as a function of fiber solid fraction, b. The predicted curve was constructed using experimental data for the porosity of each material and for particle and fiber dimensions. The error band is based on the standard deviations of these measurements.

values in Figure 10. Error bars on the experimental permeability values are also shown. It is clear that there is a good level of consistency and agreement between model (i.e., Equation (12)) and experiment, both in terms of trends predicted and values obtained.

5. Conclusions

The following conclusions can be drawn from this work, which is aimed at creating a simple capability for prediction of the permeability of a novel type of highly porous hybrid composite material designed for use as a DPF. Permeability is a key parameter for such materials, with a practical requirement that it should not fall significantly below a common industrial norm of about $10^{-2}\,m^2$. 1) A novel computational fluid dynamics (CFD) modeling technique has been developed for fiber/particle hybrid composites, with the modeled domain containing both spheres and cylinders. It has been shown to give reliable permeability predictions, based

on the porosity, the fiber solid fraction, and the dimensions of fibers and particles. For the analysis of such hybrid composites, this is an improvement over existing models, which do not allow for combinations of both fibers and particles. 2) Where the fiber diameter is smaller than the particle diameter, as in the cases treated here, the surface area increases significantly as the fiber solid fraction is raised. The surface area can be calculated from the geometry of spheres and cylinders, allowing an empirically fitted surface area correction factor to be used to account for overlap. The values obtained for the correction factor will depend on the amount of overlap allowed. Physically, this relates to the degree of sintering. 3) The most appropriate value of the Carman–Kozeny tortuosity constant, λ, was found to increase from 2 to 6.5 as porosity was raised from 0.45 to 0.7. Statistical analysis, based on data from all particle and fiber sizes

that were considered, led to the conclusion that including a linear dependence of λ on porosity is appropriate. It was found to be effectively independent of the fiber solid fraction. 4) Permeability is predicted to increase with increasing porosity for the geometry of a fiber plus particle material, as predicted by the Carman–Kozeny equation. In addition, for a constant porosity level, the permeability is found to decrease as particles are replaced by fibers. 5) A simple analytical expression has, thus, been obtained, allowing the permeability to be predicted for given levels of fiber, particulate, and porosity. It has been shown that these predictions are in good agreement with experimental data presented in a previous publication. 6) In terms of practical application as DPFs, the work provides information useful for tailoring the architecture of such hybrid material so as to avoid the permeability falling below industrial requirements. It is confirmed that this can be done while incorporating relatively high contents of fine (few μm diameter) fibers, which are thought to bring benefits in terms of both the toughness of the material and its filtration characteristics.

Acknowledgements

Conflict of Interest

The authors declare no conflict of interest.

[1] R. Prasad, V. R. Bella, *Bull. Chem. React. Eng. Catal.* **2011**, *5*, 69.
[2] J. Adler, *Int. J. Appl. Ceram. Technol.* **2005**, *2*, 429.
[3] B. Guan, R. Zhan, H. Lin, Z. Huang, *J. Environ. Manage.* **2015**, *154*, 225.
[4] J. Swanson, W. Watts, D. Kittelson, R. Newman, R. Ziebarth, *Aerosol Sci. Technol.* **2013**, *47*, 452.
[5] A. J. Houston, T. W. Clyne, *J. Eur. Ceram. Soc.* **2019**, *40*, 542.
[6] V. M. T. Su, T. W. Clyne, *Adv. Eng. Mater.* **2016**, *18*, 96.
[7] B. Formisani, *Powder Technol.* **1991**, *66*, 259.
[8] M. A. Van der Hoef, R. Beetstra, J. A. M. Kuipers, *J. Fluid Mech.* **2005**. *528*, 233.
[9] B. Markicevic, *Powder Technol.* **2019**, *350*, 154.
[10] A. Nabovati, E. W. Llewellin, A. C. Sousa, *Compos. A: Appl. Sci. Manuf.* **2009**, *40*, 860.
[11] S. Mauran, L. Rigaud, O. Coudevylle, *Transp. Porous Media* **2001**, *43*, 355.
[12] F. J. Valdes-Parada, J. A. Ochoa-Tapia, J. Alvarez-Ramirez, *Phys. A: Stat. Mech. Appl.* **2009**. *388*, 789.
[13] X. M. Chen, T. D. Papathanasiou, *Compos. A Appl. Sci. Manuf.* **2006**, *37*, 836.
[14] K. Yazdchi, S. Srivastava, S. Luding, *Int. J. Multiphase Flow* **2011**, *37*, 956.
[15] B. R. Gebart, *J. Compos. Mater.* **1992**, *26*, 1100.
[16] T. S. Lundstrom, B. R. Gebart, *J. Compos. Mater.* **1995**, *29*, 424.
[17] A. J. Houston, *PhD Thesis*, University of Cambridge **2019**.